Demonstration of broadband contrast at 1.2 λ/D for the EXCEDE Phase-Induced Amplitude Apodization Coronagraph

Dan Sirbu[a], **Sandrine J. Thomas**[b], **Ruslan Belikov**[a], **Julien Lozi**[a,b], **Eduardo Bendek**[a], **Eugene Pluzhnik**[a], **Dana H. Lynch**[a], **Troy Hix**[c], **Peter Zell**[a], **Glenn Schneider**[d], **Olivier Guyon**[d]

[a]NASA Ames Research Center, Moffett Field, CA
[b]Large Synoptic Space Telescope, Tucson AZ
[c]Lockheed Martin Space Systems Company, Palo Alto, CA
[d]University of Arizona, Tucson, AZ

Abstract. The proposed coronagraph instrument on the EXCEDE mission study uses a Phase-Induced Amplitude Apodization (PIAA) coronagraph architecture to enable high-contrast imaging of circumstellar debris disks and giant planets at angular separations as close in as the habitable zone of nearby host stars. We report on the experimental results obtained in the vacuum chamber at the Lockheed Martin Advanced Technology Center in 10% broadband light centered about 650 nm, with a median contrast of 1×10^{-5} between 1.2 and 2.0 λ/D simultaneously with 3×10^{-7} contrast between 2 and 11 λ/D between 2 and 11 λ/D for a single-sided dark hole using a deformable mirror (DM) upstream of the PIAA coronagraph. The results are stable and repeatable as demonstrated by three measurements runs with DM settings set from scratch and maintained on the best 90% out of the 1000 collected frames. We compare the reduced experimental data with simulation results from modeling observed experimental limits; performance is consistent with uncorrected low-order modes not estimated by the Low Order Wavefront Sensor (LOWFS). Modeled sensitivity to bandwidth and residual tip/tilt modes is well-matched to the experiment.

Keywords: high contrast imaging, PIAA, coronagraph, broadband, exoplanets, inner working angle, EXCEDE.

Address all correspondence to: Dan Sirbu, NASA Ames Research Center, Moffett Field, Mountain View, CA, 94035; dan.sirbu@nasa.gov

1 Introduction

The EXoplanetary Circumstellar Environments and Disk Explorer (EXCEDE) is a proposed Explorer mission concept.[1] EXCEDE was selected by NASA as a Category III laboratory investigation for an experimental demonstration of the underlying high-contrast imaging technology fulfilling part of the second goal in the Astro2010 Decadal Review to mature the technology capability for direct imaging of exoplanets.[2]

The EXCEDE mission is a science-driven technology-pathfinder. It uses a 0.7 m diameter off-axis three-mirror anastigmat telescope, and thus an unobscured pupil, that images in two 20%-wide bands at 0.4 and 0.8 µm. The main technological challenge of the coronagraph instrument is to
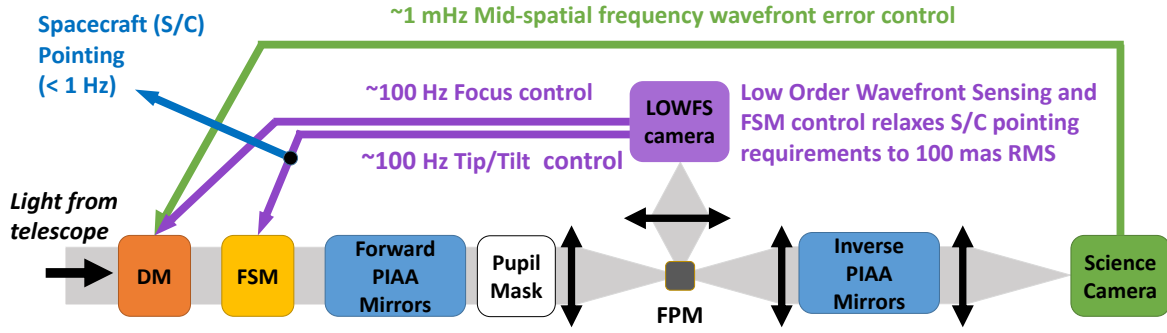
Fig 1: Block diagram of the EXCEDE Starlight Suppression System. A Low Order Wavefront Sensor (LOWFS) camera is used in conjunction with a Deformable Mirror (DM) and a Fast Steering Mirror (FSM) to remove low-order modes upstream from the Phase-Induced Amplitude Apodization (PIAA) coronagraph. The PIAA coronagraph consists of forward PIAA mirrors with a Focal Plane Mask (FPM). Inverse PIAA mirrors enable a wide field of view. The wavefront correction loop using estimates from the science camera generates a dark hole in the image plane enabling high-contrast imaging.

achieve a high-level of contrast at a small angular separation from the host star (on the order of 100 mas for a star at 10 pc). The EXCEDE coronagraph instrument uses a starlight suppression system (SSS) and has a science-driven 10^{-7} raw contrast requirement for an angular separation between 2 and 22 λ/D and 10^{-6} raw contrast from 1.2 to 2 λ/D. These capabilities enable EXCEDE's primary science mission goals to directly image and characterize the circumstellar environment in habitable zones consisting of dust disks and giant planets.

The proposed EXCEDE SSS is shown in block-diagram form in Figure 1 and its function is to enable high-contrast imaging at small angular separations. Two fundamental physical phenomena prevent direct imaging of an exoplanet with a space telescope: diffraction and internal scattering.

First, diffraction of the central starlight for an unobscured aperture creates the well-known Airy disk point spread function (PSF) whose rings are several orders of magnitude brighter than the science targets which are thus obscured. The key component of the SSS is a set of two specially-shaped mirrors that act as a Phase-Induced Amplitude Apodization (PIAA) coronagraph. The sur-

face curvature of these PIAA mirrors reshape the input light beam to a more favourable apodization that reduces the diffraction rings of the PSF.[3] A focal plane occulter blocks the central core of the PSF providing starlight suppression and further improving contrast in the focal-plane region of interest. The PIAA architecture reshapes and does not block the pupil, thus all the planet light is propagated through the coronagraph and the design is highly efficient. This increased efficiency allows using a relatively smaller telescope diameter for the equivalent science of a telescope with a larger diameter, and is the main driver for the small-scale size of the EXCEDE mission. A set of Inverse PIAA mirrors introduce a reverse mapping of the pupil in order to recover a wide-field of view.[4]

Second, there is light scattering inside the telescope. Manufacturing limitations on all the optical surfaces result in static and quasi-static mid-spatial frequency wavefront errors that introduce speckles in the image plane. The wavefront control (WFC) system is shown in orange and green and consists of the science camera and a Deformable Mirror (DM). Using focal-plane sensing at the science camera the wavefront error can be estimated and fed to the Deformable Mirror (DM) forming a WFC loop to correct wavefront errors and create regions of high-contrast in the image plane called dark holes. Finally, environmental disturbances and instabilities on the spacecraft for example due to internal vibrations and temperature gradients are measured and controlled by the Low Order Wavefront Sensor (LOWFS) system shown in purple, orange, and yellow. A high-frequency camera uses the PSF core reflected from the focal plane mask to estimate the low-order modes with tip/tilt and corrected by a fast-steering mirror (FSM) and defocus corrected by the DM. This represents a second control loop that stabilizes the wavefront operating at a higher frequency than the speckle removal loop. Finally, the resulting dark hole in the image plane is formed on the science camera, which is a two-band Nyquist sampled imaging polarimeter.

In this paper, we report on the laboratory investigation that was carried out in a vacuum chamber facility at the Lockheed Martin Advanced Technology Center as part of the technology maturation for the EXCEDE mission concept. The main contribution in this paper is the experimental demonstration of the PIAA coronagraph at a very aggressive inner working angle of 1.2 λ/D in 10% broadband light for a bench operating in a flight-like configuration. More specifically, this laboratory demonstration reports 1.0×10^{-5} raw median contrast between 1.2 to 2.0 λ/D simultaneously with 3.0×10^{-7} median contrast between 2.0 to 11.0 λ/D. In this paper, we present:

- a description of the experimental facility, the configuration of the optical bench, and the alignment procedures (**Section** §**2**),

- a summary of the experimental results demonstrating repeatability and stability through three separate runs (**Section** §**3**),

- a comparison to models through a sensitivity analysis to identify the limiting factors in the experimental demonstration (**Section** §**4**),

- concluding remarks summarizing the experimental results, the understanding of the limiting factors, and possible steps to improve contrast performance (**Section** §**5**).

To place the current experimental investigation in context, we provide a comparison with other experiments that have been completed or are on-going. A coronagraph instrument on the WFIRST-AFTA mission is currently under study and accelerated technological development. A Phase-Induced Amplitude Apodization Complex-Mask Coronagraph (PIAACMC) has been selected as an alternative option to the primary Occulting Mask Coronagraph (a dual-mode Shaped Pupil and Hybrid Lyot that share the same architecture). The PIAA coronagraph and technology maturation

4

for the EXCEDE mission concept is relevant for the WFIRST-AFTA PIAACMC coronagraph, and is complementary with the on-going experimental demonstrations of the Occulting Mask Coronagraph. Whereas the WFIRST-AFTA coronagraph is expected to achieve a deeper contrast, the EXCEDE coronagraph would operate at both a smaller inner working angle and wider outer working angle.

The first PIAA coronagraph system laboratory validation took place at the Subaru Telescope[5] – this investigation reported a 2.3×10^{-7} raw contrast for a single-sided region between 1.65 to 4.4 λ/D operating in air with monochromatic light and without inverse PIAA mirrors. A PIAA lens system then has first been used in a temperature-stabilized testbed in air at the NASA Ames Coronagraph Experiment[6] resulting in 5.4×10^{-8} monochromatic raw contrast from 2.0 to 5.2 λ/D. The best raw contrast achieved using a PIAA system were obtained on the same testbed with reflective PIAA mirrors (also without an inverse PIAA system) with 1.9×10^{-8} raw contrast from 2.0 to 3.4 λ/D and 1.2×10^{-6} raw contrast from 1.5 to 2.0 λ/D in monochromatic light.[7] Most recently, a PIAA coronagraph was used at the NASA JPL High-Contrast Imaging Testbed in 10% broadband light from 2.0 to 4.0 λ/D recording 10^{-8} raw contrast.[8]

Other coronagraph systems have achieved deeper contrasts but at larger inner working angles. As part of the WFIRST-AFTA technology demonstration, the Shaped Pupil Coronagraph testbed has recently reached its monochromatic milestone reporting 6.0×10^{-9} raw contrast from 4.4 to 11.2 λ/D including the unfavourably obscured AFTA pupil.[9] Similarly, the Hybrid Lyot Coronagraph demonstration obtained 8×10^{-9} raw contrast from 3.0 to 9.0 λ/D in a 360 degree dark hole for the AFTA pupil.[10] Numerical studies have shown that the PIAACMC coronagraph mode with the AFTA pupil has the potential for an increase in science yield due to its smaller inner working angle and increased throughput,[11] but it can be sensitive to low-order aberrations (especially

line-of-sight jitter).[12] To date complex phase masks have only been recently manufactured[13] and off-axis PIAACMC mirrors have been designed,[14] with laboratory investigations planned in the future.

We emphasize that the results presented in this paper represent the smallest inner working angle demonstration to date (operating down to 1.2 λ/D), are conducted up to 10% broadband light, and are a realistic implementation of the proposed EXCEDE coronagraph instrument.

2 Laboratory Configuration

The laboratory investigation we present in this paper is the final in a series of demonstrations that were all part of the EXCEDE technology maturation process for the PIAA-based starlight suppression system. The earlier technology demonstrations were first carried out in the temperature-stabilized testbed at the NASA Ames Coronagraph Experiment using only forward PIAA mirrors,[15,16] and subsequently incorporated the first operation of the fast Low Order Wavefront Sensor.[17,18] In this paper, we will focus exclusively on high-contrast results obtained in a vacuum environment with an optical bench that represents the final EXCEDE-like flight configuration.[19,20]

2.1 Experiment Facility

The EXCEDE laboratory demonstration was carried out in a vacuum chamber facility at the Lockheed Martin Advanced Technology Center. This thermal vacuum Metrology (MET) chamber is embedded in a 20 ft wide by 40 ft long (6 m by 12 m) class 1000 cleanroom. The chamber itself is 8 ft (2.4 m) wide and sufficiently tall to allow comfortable access in air to the entire length of the 4 x 20 x 2 ft (1.2 x 6.1 x 0.6 m) optical table that is integrated to the chamber through vibration isolators located external to the chamber. The entrance to the chamber is shown in Figure 2(a) and
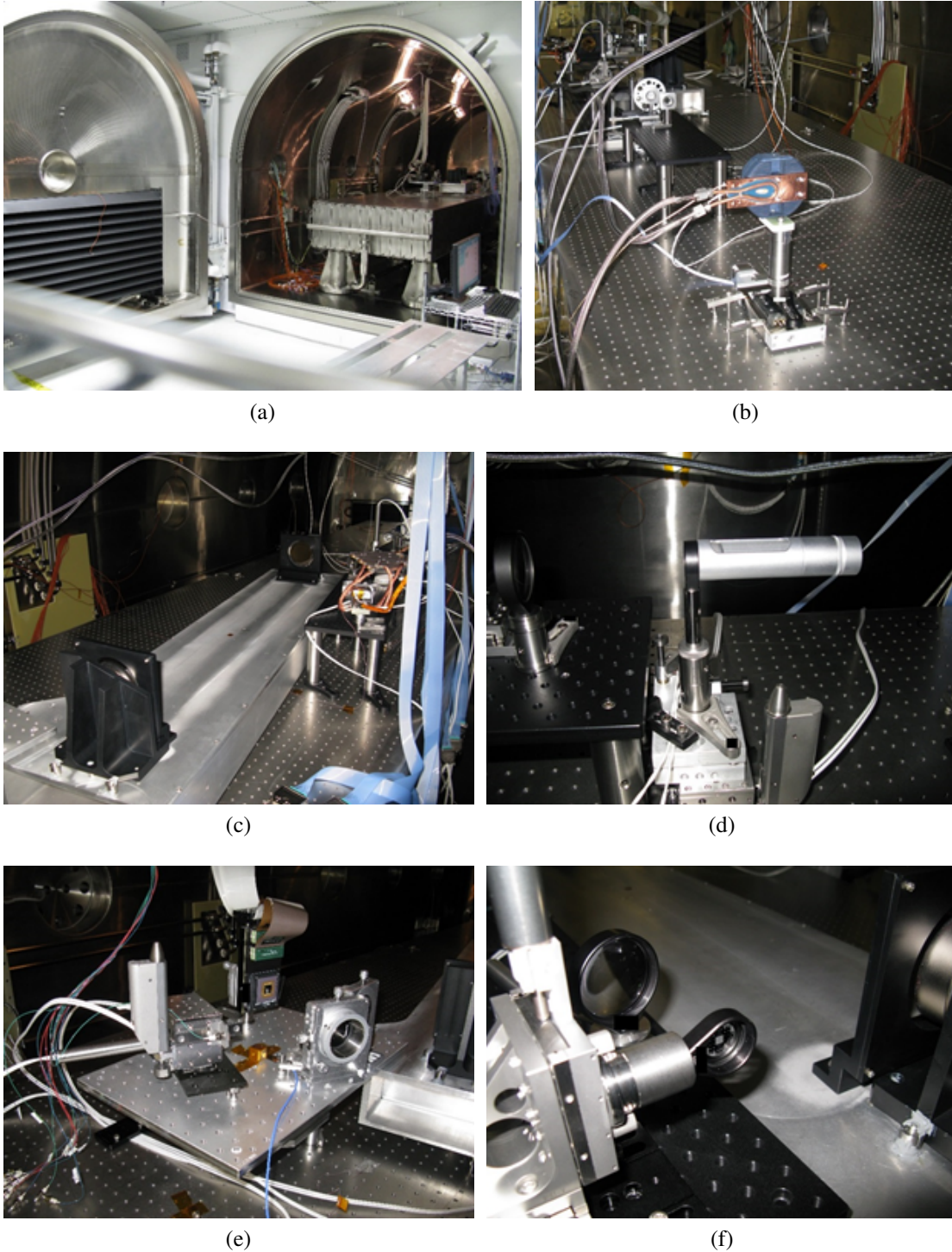
(a)

(b)

(c)

(d)

(e)

(f)

Fig 2: Experimental demonstration was performed in the vacuum MET chamber facility at the Lockheed Martin Advanced Technology Center. (a) Class 1000 clean room at the entrance of the vacuum chamber. (b) View of the EXCEDE optical testbed from the science camera end. (c) View of forward PIAA mirrors. (d) View of inverse PIAA lenses. (e) View of front-end optics on platform with two OAPs and the DM. (f) View of the focal plane mask

7

the final configured testbed are shown in Figures 2(b)-(f).

The testbed features no enclosure, as the intent is to operate in vacuum. This implies, however, that high-contrast cannot be realistically achieved in air due to an uncontrolled environment. The vacuum environment within the chamber is produced by an Edwards dry roughing pump, a cryogenic pump, a turbo molecular pump, and a liquid nitrogen getter plate. In vacuum, thermal gradients are monitored and mapped (but not controlled) with temperature probes located on important components throughout the testbed, and the cameras cooled and outfitted with heat-sinks. Environmental data consisting of pressure, temperature, vibration, and acoustic measurements are logged, and these data were analyzed in more detail as part of the presentation of the initial vacuum results.[19]

The vacuum testbed was configured over the course of five separate Vacuum Chamber Tests (VCTs) to as much as possible closely resemble the proposed EXCEDE configuration. The primary considerations for this progressive configuration were the following:

1. enabling an exploration/demonstration of contrast performance with polychromatic light with up to a 10% bandwidth vs. monochromatic light around a 650 nm central wavelength.

2. verification of a wider outer working zone, with the final verification of the outer working angle set to 11 /D.

3. demonstration of system operability in a vacuum environment.

In practical terms, the main laboratory updates to reflect these requirements were: (i) the usage of a supercontinuum white laser source with a selectable bandwidth filter for polychromatic contrast, with reflective optics used to mitigate chromatic effects and refractive optics used for less
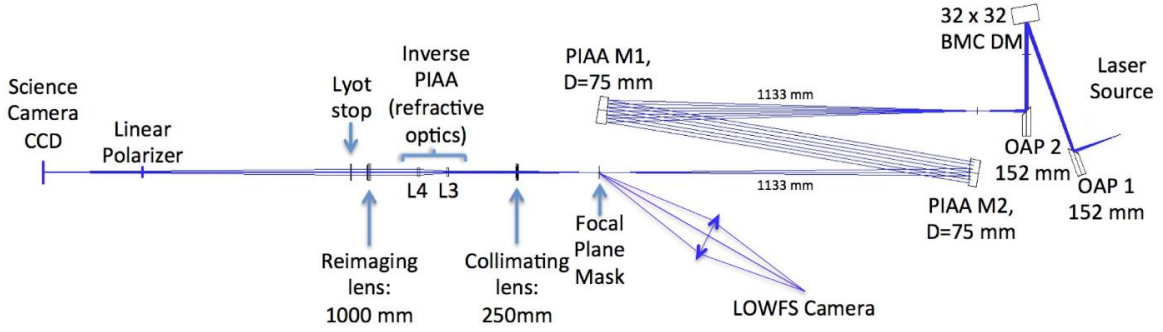
Fig 3: Optical configuration of the EXCEDE test bench.

sensitive functions, (ii) introduction of inverse PIAA optics to enable a wider field of view with an unaberated PSF in the final focal plane, (iii) a DM position upstream of the forward PIAA optics, to work in conjunction with the inverse PIAA system and to enable removal of tip/tilt modes with sensing provided by the LOWFS prior to propagation through the forward PIAA system, and (iv) preparation of electronic components and optical mounts for the testbed for vacuum compatibility.

2.2 Optical Testbed

The final optical configuration of the EXCEDE testbed for polychromatic demonstration in vacuum is shown schematically in Figure 3. The propagation of the beam from the external source input to the science camera imaging detector at the final focal plane is described below:

LASER SOURCE. The laser source used is a supercontinuum light source (an NKT photonics SuperK laser) with a variable bandwidth filter (the SuperK VARIA tunable single line filter) coupled into a single mode fiber. The single-mode fiber output is an approximation to a point-source (stellar) image delivered by a telescope, and is fed into the vacuum chamber via a port hole. The central wavelength was selected to be 650 nm due to being in the optical region and a compromise of the two proposed EXCEDE bands. All the optics upstream from the focal plane mask are reflective to mitigate chromatic effects. All refractive optics are located after the focal plane mask to

9

ensure their aberrations do not impact the ability of the focal plane mask to suppress the on-axis stellar PSF and, additionally, are all placed in a slow beam.

OAPs. The laser source feeds front-end optics containing the DM that was positioned upstream of the forward PIAA system mimicking the EXCEDE flight architecture. The front-end optics are shown in Figure 2(e). Two OAPs, with $\lambda/4$ surface quality, are used to: (a) create a point focus input to the forward PIAA with an f/15 beam, and (b) conjugate the DM with respect to the first forward PIAA mirror (M1).

DM. The DM used is a 32x32 actuators Boston Micromachines MEMS. The DM is conjugated to PIAA M1 to avoid geometrical distortion effects due to the forward PIAA system and allow for wide field correction. The DM converts commanded voltages into displacement of individual actuators. An iterative speckle-nulling (SN) wavefront correction algorithm was used to compute the DM settings creating the high-contrast region in the image plane.

FORWARD PIAA MIRRORS. The beam next propagates to the forward PIAA mirrors shown in Figure 2(c). These are the same first-generation Axsys PIAA mirrors used in the Subaru,[5] JPL,[8] and earlier EXCEDE results.[16,19] They were not specifically optimized for broadband performance using a 1.2 λ/D focal plane mask and were instead used as-is.

FOCAL PLANE MASK. The focal plane mask, with a photograph shown in Figure 2(f) and a schematic shown in Figure 7(b), is at the prime focus of the forward PIAA system. The focal plane mask has a C-shape deposit on glass with a reflective circular inner occulter blocking the core of the PSF. The light reflected from the inner circular occulter feeds to the LOWFS. A straight edge blocks one entire side of the focal-plane, and an outer circle blocks light at off-axis angles greater than 16 λ/D.

LOWFS. The central core of the PSF is reflected by the focal plane mask to the LOWFS

system. A re-imaging lens is used to form a slightly defocused image on the LOWFS camera. A 14-bit ImperX Bobcat ICL-B0620 provides a high frame rate and a National Instruments PXI controller establishes a real-time control loop with the DM. The design, performance and operation of the EXCEDE testbed LOWFS is detailed in earlier reports.[17,18] We emphasize that only the tip/tilt modes are estimated and corrected in this experiment. Additionally, the correction loop is closed with appropriate settings set on the DM.

INVERSE PIAA LENSES. The inverse PIAA lenses are shown in Figure 2(d) and are placed in a collimated space in order to reduce refractive effects in polychromatic light. As these lenses are located after the FPM, their aberrations do not impact the ability of the FPM to suppress the on-axis light.

LYOT STOP. A Lyot stop is placed shortly after a final re-imaging lens, and thus in nearly collimated space. This defines the exit pupil and blocks out the edges of the second pupil plane diffracted light. The light blocked by the Lyot stop is high-spatial frequency and is due to to the focal plane occulter's edge diffraction effects.[7]

LINEAR POLARIZER. Earlier experiments have shown that in the contrast regime that the EXCEDE experiment operates polarization effects become a limiting factor particularly in the outer working zone.[7] A linear polarizer is therefore located immediately prior to the science camera and mitigates any instrumental polarization effects due to reflective optics in the system.

SCIENCE CAMERA. The science camera, located in a re-imaged focal plane after the linear polarizer, is used both for target imaging, and for closed loop mid-spatial frequency wavefront sensing and control with the DM. It has an as-calibrated linear image scale of 5.5 pixels per 1 λ/D. This 16-bit QSI 520i series CCD camera provides a low read-noise output and is shown in Figure 2(b). It has a regulated thermoelectric cooler which is maintained at 1 C to avoid ice crystal

formation during operation. We discovered contaminant deposition on both the exterior vacuum window and the surfaces of the CCD window (a few mm ahead of the final focal plane) during in-air preparatory activities before the final VCT. These manifested as slightly afocal (diffractive) spots on the science camera image. Removal of the vacuum window eliminated the largest-sized diffraction spots. The contaminant on the internal surface of the CCD window resulted in remaining small nucleation spots and can be seen in the final reduced experimental figures (see the reduced images in Table 1). We did not find that this negatively affected the SN WFC algorithm or calibration procedures.

2.3 System Calibration

In order to ensure repeatability and accuracy of the system, the EXCEDE bench uses an automated calibration procedure to align the various components of the system. This is an important part of the experimental procedure and useful for vacuum operation when the system is inaccessible. Operation of the bench is run via a LabVIEW GUI, which is shown in Figure 4. The LabVIEW GUI is able to launch different procedures which align the different parts of the system and calibrate the system model; when all the alignment procedures have been completed it is possible to start the iterative WFC algorithm. Here we summarize the main calibration procedures used on the bench during each demonstration run:

INPUT FIBER ALIGNMENT: The input fiber is aligned in both orthogonal directions (X, Y) in the transverse plane with respect to the optical axis, to assure on-axis concentricity with respect to both the front-end optics, and to the PIAA system. Due to the inverse PIAA optics, the science camera is not a good candidate for a measurement of this alignment. Instead, the PSF core reflected light from the FPM is imaged on the LOWFS camera. A sharpness metric defined as
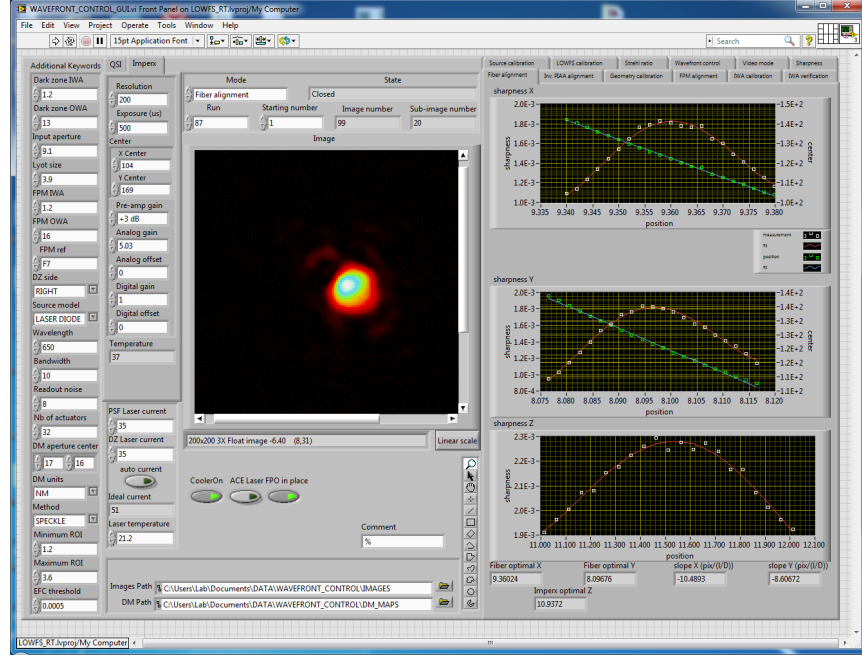
Fig 4: System calibration is controlled via a LabVIEW GUI. Here the input fiber alignment mode is selected, with other alignment modes accessible via indicated tabs.

$\Sigma = \text{image}^2/(\Sigma\text{image})^2$ over all PSF pixels on the LOWFS camera is maximized while the fiber is moved both along the X- and Y-axes. The LOWFS camera is set at a slightly defocused location to remove degeneracy. The procedure is iterative and run until the optimal locations are stable.

INVERSE PIAA ALIGNMENT AND IMAGE SCALE: The location of the inverse PIAA lenses must be separately aligned to ensure on-axis concentricity with respect to the forward PIAA mirrors and the front-end optics. Additionally, the best-focus location for the science is established, and the image scale in terms of pixels per λ/D at the science camera image plane is measured. The FPM is moved out of the way to ensure the unocculted PSF is visible on the science camera. The inverse PIAA lens is moved along both transverse axes (X, Y), and the maximal sharpness locations are maintained. The science camera is also moved along the optical axes (Z) to ensure the best focus. The fiber is displaced a known amount along both X and Y to determine the final image plane scale.

13

CONTRAST CALIBRATION: An unocculted reference image of the PSF of the aligned system is obtained at the same central wavelength used for the Wavefront Control iteration algorithm. The FPM is moved to allow the PSF to pass through a transparent part of the mask. The unocculted, unsaturated PSF is recorded and the peak flux density is ratioed to every pixel to obtain contrast-calibrated images. For broadband contrast images, the science camera saturates at the shortest possible available exposure times (and reducing the overall intensity would significantly increase the duration of each wavefront control iteration). We therefore used integrated measurements of the flux from the reflected core light on the LOWFS camera for both the monochromatic and broadband PSFs to obtain the necessary calibration ratio.

FPM ALIGNMENT: To ensure that the C-shaped focal plane occulter mask was correctly aligned and positioned the FPM was moved along both transverse axes (X, Y). At each location the total energy in the image obtained was summed, and divided with respect to the energy in the unocculted PSF. Along the Y axis (coinciding with the masks straight edge), the relative energy was minimized; along the X axis the FPM location was chosen such that the relative energy was 50%.

IWA VERIFICATION: A separate procedure was used to verify the location of the C-shaped occulter without the necessity of re-alignment of the occulter (i.e., to ensure that hysteresis does not result in a different FPM location). Instead, the fiber was displaced along the X axis by known amounts and the relative energy was measured. This process assures that the PSF was not moved by tilts introduced on the DM by the wavefront control algorithm, and that no other changes in the system affected the location of the IWA. The verification procedure has $\pm 0.05\lambda$/D uncertainty.

LOWFS CALIBRATION: The LOWFS uses reflected light from the focal plane mask. The core of the reflected PSF from the circular inner part of the C-shape mask is focused onto a high

frame-rate camera. For calibration, a reference image of the reflected PSF is constructed by collecting an initial set of images from the LOWFS. Subsequent images are subtracted with respect to the reference image and the shifted centroid is computed. A known set of tip/tilt modes are applied to the DM to construct an influence matrix with respect to the LOWFS focal plane.

3 Experimental Results

In this section, we report on the demonstration of polychromatic contrast in the vacuum chamber carried out as part of the final VCT. The geometry of the dark zone can be seen in Figure 5, with an Inner Working Zone (IWZ) defined between 1.2 and 2.0 λ/D and Outer Working Zone (OWZ) between 2.0 and 11.0 λ/D. Furthermore, the experimental measurements were demonstrated in a precisely defined and repeatable fashion. To demonstrate repeatability the experimental measurements is taken three times. The bench is recalibrated via the automated LabVIEW procedures and DM settings are set to scratch for each run. To demonstrate stability, each such run needs to hold over at least 1000 collected frames with the best 90% frames used to compute the median contrast.

The demonstration is performed in 10% bandwidth centered about 650 nm. Initially, the system calibration and Speckle Nulling (SN) WFC iterations are performed at the smallest selectable filter bandwidth available on the VariaK (10 nm). The LOWFS is engaged once the IWZ contrast limit is reached – this particular limit is 1×10^{-5} in the 10 nm narrowband wavelength, and without the LOWFS a better IWZ contrast cannot be reached. The final IWZ contrast achieved in 10 nm is 3×10^{-6}. Once contrast has stabilized, we increase the bandwidth to 65 nm (i.e., 10% bandwidth) and measure the resulting polychromatic contrast. The results from each of the three separate runs are summarized below in Table 1.

For each of the three test runs characterized in Table 1 a single, but typically representative,
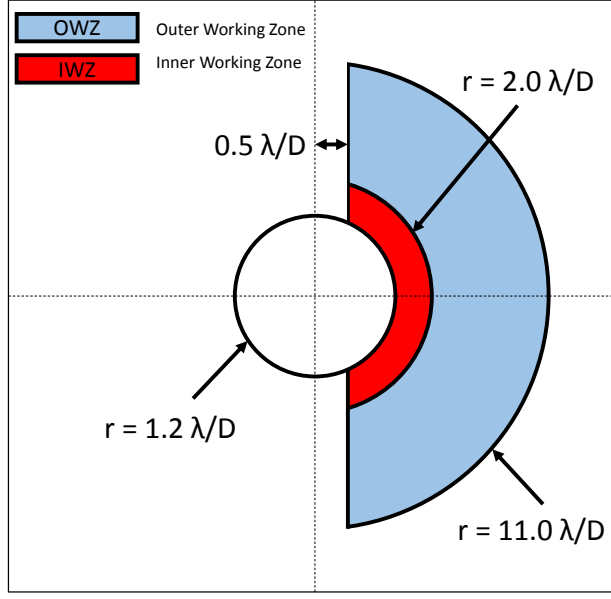
15

Fig 5: Dark hole definitions for EXCEDE measurements. Inner working zone (IWZ) is defined between 1.2 and 2.0 λ/D and Outer Working Zone (OWZ) is between 2.0 and 11.0 λ/D.

contrast field image (from the ≥ 1000 obtained) is shown under the Image column. The individual images are highly repeatable, as evidenced in the contrast stability plots shown under the Stability column for each test presenting the raw median contrast metric as a function of image iteration. In all three cases, data were collected with the establishment of the dark zone by SN for ≥ 1000 iterations, as follows:

- In Test A (top panels), 2,000 images were collected contiguously with a time-averaged cadence of one frame every 2 seconds (over 67 minutes).

- In Test B (middle panels), we took the opportunity to test the longer term stability of SN by continuously taking data over ~ 14 hours. We began with 1,500 images collected similarly to Test A. Then, without resetting the DM, we explored broadband performance at other bandwidths (from 50 nm to 10 nm, not illustrated here, but compared with models in Section
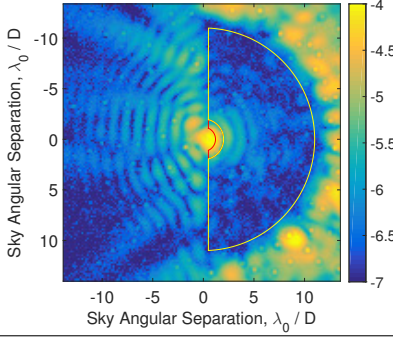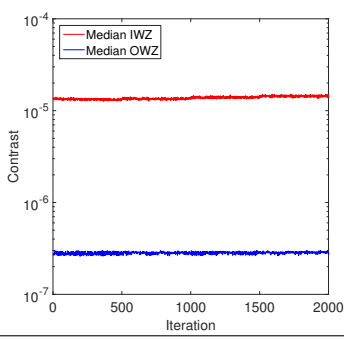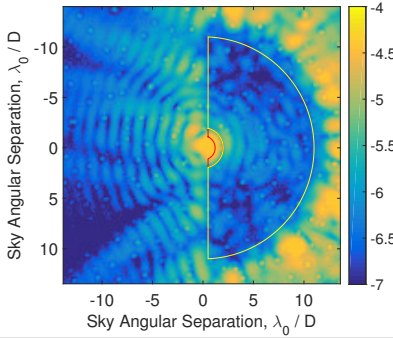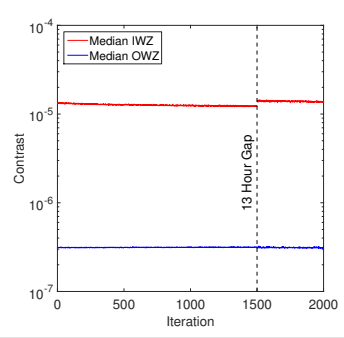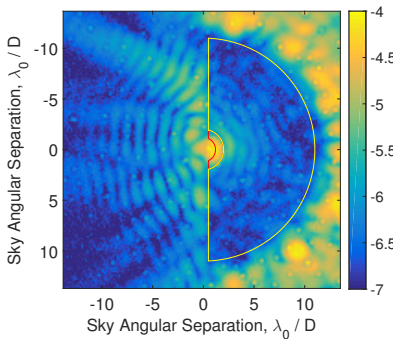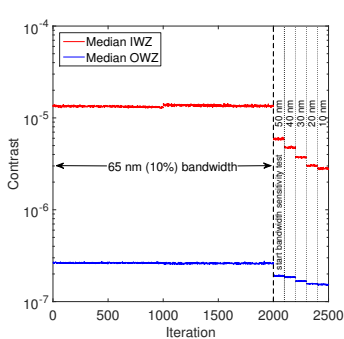
Summary	Image (Raw Contrast)	Stability over $1000 \geq$ iterations
Test A Time interval: 67 mins Mask position: 1.2 λ/D λ_{central} = 650 nm Bandwidth = 10% Median raw contrast: 1.2-2.0 λ/D: 1.35×10^{-5} 2.0-11 λ/D: 2.82×10^{-7}		
Test B Time interval: 816 mins Mask position: 1.2 λ/D λ_{central} = 650 nm Bandwidth = 10% Median raw contrast: 1.2-2.0 λ/D: 1.29×10^{-5} 2.0-11 λ/D: 3.14×10^{-7}		
Test C Time interval: 61 mins Mask position: 1.2 λ/D λ_{central} = 650 nm Bandwidth = 10% Median raw contrast: 1.2-2.0 λ/D: 1.33×10^{-5} 2.0-11 λ/D: 2.63×10^{-7}		

Table 1: Summary of the three experimental runs for the demonstration of 10% bandwidth starlight-suppression: 1.2 to 11 λ/D at 650 nm. The small nucleated spots on the experimental images are contaminant deposition on the inside of the science camera CCD window from out-gassing in the vacuum environment.

§4) before contiguously collecting another 500 images at 65 nm (corresponding to 10 % bandwidth). The stability of the SN-established WFC over that period of time is evidenced by the contrast metrics at 10% bandwidth that are graphed (collapsed across the 13-hour gap

when data were being taken at other bandwidths) in the column on the right.

- In Test C (bottom panels) was executed similarly to Test B, but with 2,000 images at 65nm
  (10%) bandwidth taken with different exposure times (1000 images with 0.1 s exposures,
  followed by another 1000 iterations with 0.14 s exposures). We use those 2,000 images
  for our 10% bandwidth contrast metrics. Following that, as in test B, the bandwidth was
  incrementally decreased in consecutive iterations, in this case, of 100 images each that are
  shown here for illustrative purposes only. The 65 nm (10%) bandwidth results are virtually
  identical to Tests A and B in the OWZ.

4 Sensitivity Analysis

To better understand the physical limitations of the as-implemented testbed, and in particular to
identify the factor(s) limiting the experimental performance informed by experimental test results,
specifically at the smallest stellocentric angle in the Inner Working Zone (IWZ) between 1.2 and
2.0 λ/D, we provide here in detail a description of, and the results from a performance sensitivity
analysis.

4.1 Model Description

We have adopted a geometrical remapping optical propagation model between the PIAA mirrors
and with all the optical planes in the system modeled defined as Fourier conjugates. Despite its rel-
ative simplicity, the model replicates the observed performance (and limitations) of the experiment
quite well (as we will demonstrate). This model of the EXCEDE testbed coronagraphic optics is
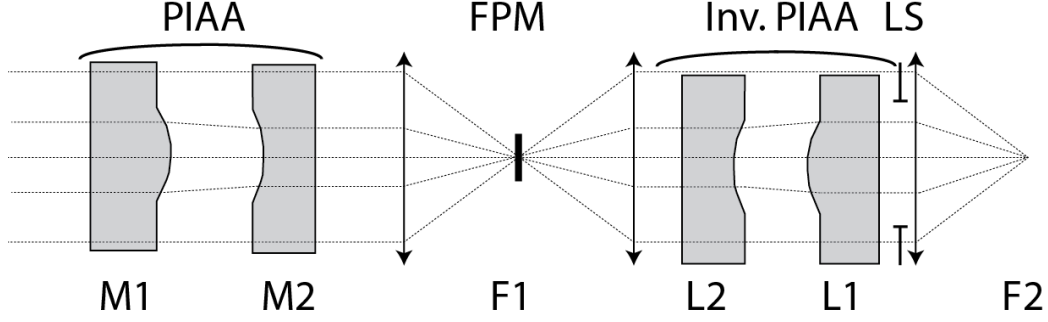schematically illustrated at a high level in Figure 6.

Fig 6: Optical element and plane definitions for the optical model employed. The forward PIAA consists of the two mirrors M1 and M2 (illustrated only for simplicity as transmissive optics). The Focal Plane Mask (FPM) is located at the first focal plane F1. The Inverse PIAA consists of two inverse lenses L2 and L1. A Lyot stop (LS) is located at the exit pupil, and the final science image is formed at the re-imaged focal plane F2.

The EXCEDE layout contains forward PIAA coronagraphic optics with two mirrors. These mirrors are defined by two planes at M1 and M2. The propagation between M1 and M2 is defined in our model by a ray-tracing pupil-mapping function. The intensity at the forward PIAA exit pupil (M2) is shown in Figure 7(a). The DM is physically located upstream of the PIAA system and in the simulation this is approximated as the DM being conjugate to M1.

The C-shaped Focal Plane Mask (FPM) as shown in Figure 13 (right), is located at the first focal plane F1. The propagation between the exit PIAA pupil at M2 and the entrance pupil of the first inverse PIAA lens at L2 is performed using a convolution operation (with a Fourier transformation of the FPM). The inverse PIAA lenses at L2 and L1 perform an inverse pupil-remapping operation to the forward PIAA mirrors also modeled through ray-tracing. At the exit pupil of the inverse PIAA system, a Lyot stop blocks diffracted light from the focal plane mask. The physical dimension of the PIAA system, the corresponding magnification and sizing of the focal plane mask, the open diameter of the Lyot stop, and the pixel sampling at the final science plane are all

matched to the experimental testbed.

All optical aberrations are collocated at the entrance pupil of the system, the M1 plane, and are propagated through the system as described. These aberrations can be corrected with the DM using either the iterative Electric Field Conjugation (EFC) or Speckle Nulling (SN) wavefront control algorithms. As in the VCT 5 demonstration, in simulation the WFC are applied for the central wavelength of 650 nm, the DM setting is maintained, and the input light bandwidth is extended to $\lambda_{\text{central}}/\Delta\lambda = 10\%$. This procedure follows the experimental correction.

The geometrical remapping method has been validated against other PIAA propagators (geometrical remapping with Talbot effect correction which simulates diffraction, Fresnel diffraction, S-Hyugens diffraction) with the following conclusions: for on-axis modes with no errors, geometrical remapping gives the same result (down to 10^{-10} level) as long as the edges of the pupil are feathered with a pre (or post-) apodizer. Without apodizers, the results are correct to the 10^{-7} contrast level of this experimental demonstration. For low-order modes (tip/tilt, defocus, etc) the results are similar. For higher order modes, the shape of the speckle field in the focal plane starts deviating between geometrical remapping and other models, but the contrast levels remain the same. Therefore, for purposes of determining contrast of the speckles (as opposed to exact morphology), geometrical remapping is a sufficient model for the contrast levels at which the first-generation PIAA system used in this experiment operates.

4.2 Ideal Performance

To establish a baseline against which to compare the observed limitations of the experiment, we simulate the performance of the system first under ideal conditions. This involves generating only a pure $\lambda/20$ phase aberration with a decreasing frequency ramp ($1/f^{3/2}$) in amplitude and
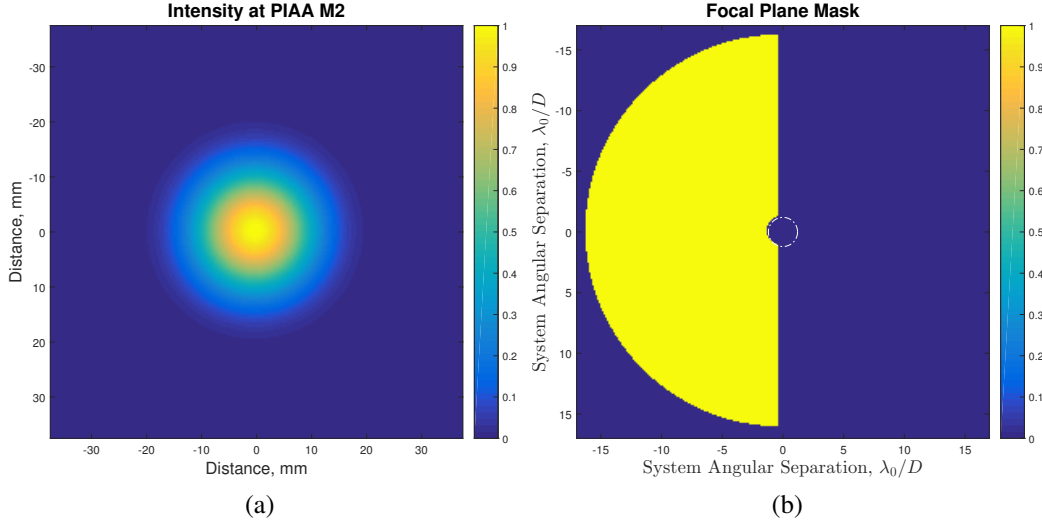
Fig 7: (a) The simulated PIAA pupil (M2 plane) (b) The one-sided C-shaped focal plane mask.

assuming the circular occulter of the focal plane mask is completely opaque. In this idealized case, the starting contrast in the dark hole region is limited only by speckles caused by relatively high frequency scattering giving rise to a PSF with a near-unity Strehl ratio of 0.99. The result of this ideal case for 10% broadband light is shown in Figure 8. Thus, the median contrast under ideal conditions in 10% light is 2.06×10^{-6} from 1.2-2.0 λ/D (IWZ) and 1.69×10^{-8} from 2.0-11 λ/D (OWZ). We have compared both Speckle-Nulling (SN) and Electric-Field Conjugation (EFC) wavefront correction to ensure results are not algorithm-limited and obtained near-identical final performance. Introduction of experimental limitations will worsen contrast performance compared to this ideal level.

4.3 Low Order Aberrations

The EXCEDE starlight suppression system has a LOWFS to measure low-order aberrations with commands sent to the DM for their correction. In this technology demonstration, the low-order aberrations that are sensed and corrected are the tip/tilt modes. In ex post-facto model simulations, we introduce phase aberration modes in proportions that match the shape of the experimental PSF.
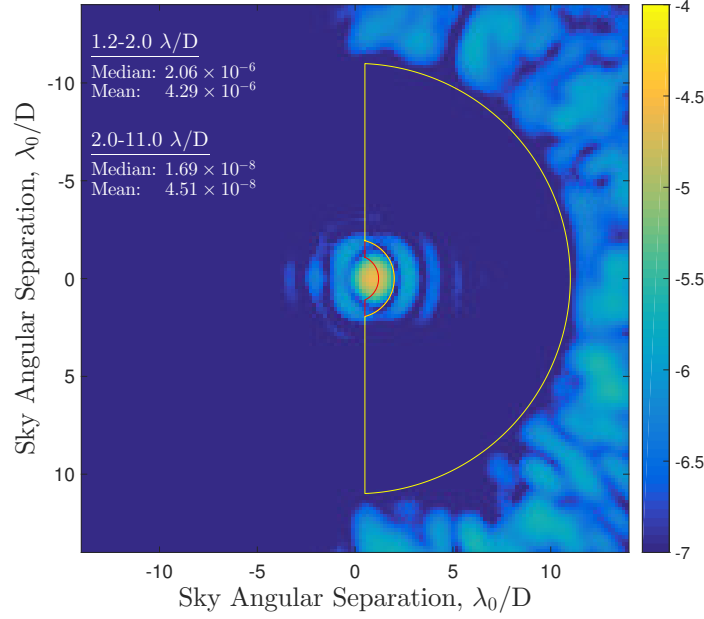
Fig 8: Ideal performance of EXCEDE starlight suppression system in simulation with closed-loop wavefront correction. The theoretical best performance in the IWZ and OWZ for the EXCEDE laboratory bench is computed in terms of both median and mean raw contrast.
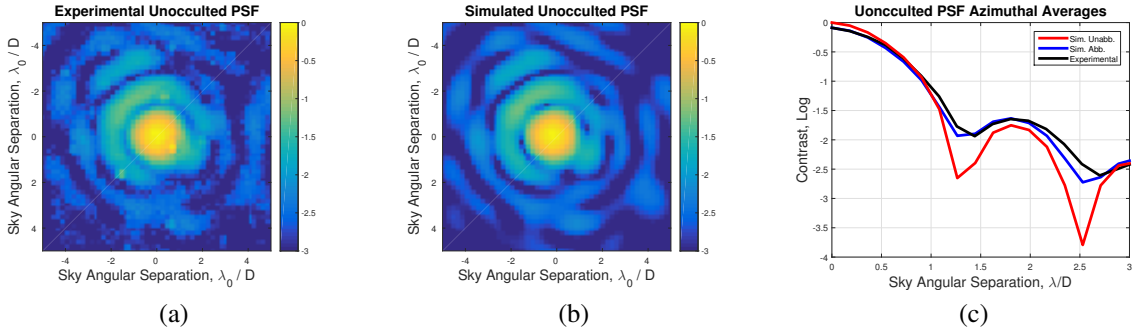

Fig 9: (a) Experimentally measured on-axis PSF without an occulter (SR = 0.81) (b) Simulated on-axis PSF matched to the experimental PSF (c) Azimuthally averaged profiles of the unocculted PSFs comparing the unabberated simulated system (red and blue curves respectively) and the best-matched aberrated simulated system with the experimental results (black curve).

This is achieved by applying the Gerchberg-Saxton algorithm to compute an estimate of the net phase aberrations through the entire system.

In Figure 9, we compare images of the experimental PSF in (a) with the corresponding simulated PSF (b) – both represent the on-axis, unocculted case. The simulated PSF corresponding to the estimated aberrations phase-map corresponds to a Strehl Ratio (SR) of 0.81 which matches

experimental Strehl measurements taken during alignment (0.8-0.85). We also show in the right-pane 360-degree azimuthally averaged radial profiles of the experimental and simulated PSFs. The red-curve represents the unaberrated theoretical (ideal) PSF of the system. There is very good agreement especially for the lower-order portion of the PSF between the simulated aberrated PSF and the experimental PSF as seen by comparison of the corresponding blue and black curves.

The resulting total phase aberration map across the entire optical system is shown in Figure 10. These aberrations correspond to RMS amplitude of 0.4 radians, and a combination of these is applied at both the PIAA entrance pupil (M1) and the Inverse PIAA exit pupil (L1). Fitting Zernike polynomials to these phase aberrations shows that they are dominated by the first 30 Zernike polynomials, with the presence of primary and secondary astigmatism resulting in a good match of the diffracted light beyond the focal plane mask. The cause of these astigmatic aberrations remains somewhat speculative. We suggest that the most likely source is due to misalignment between the front-end OAPs. The optical alignment of the testbed was performed in air, then tested in vacuum, and misalignment (particularly between the OAPs) plausibly was introduced by the change of environment from air to vacuum.

We then perform a sensitivity analysis with respect to a residual tip/tilt term. No tip/tilt terms were added with the low-order aberrations, but after performing wavefront control and obtaining an optimal DM setting we add residual tip/tilt to determine the robustness of the solution to small tip/tilt deviations. Because of the number of iterations involved in a typical experimental run and the integration times, it is likely that some residual misalignment may develop. The results of the sensitivity to residual tip/tilt are shown in Figure 11(a). We plot both the monochromatic (1.5 % banwidth) and the broadband simulated sensitivity contrast curves for both the IWZ and OWZ. We compare the simulated contrast IWZ contrast curve to an experimental sensitivity test
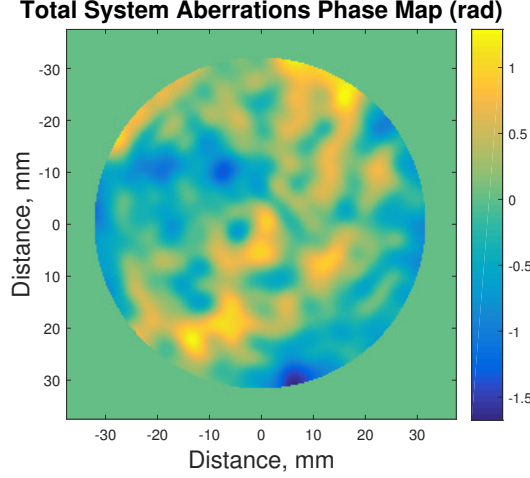
Total System Aberrations Phase Map (rad)

Fig 10: Phase aberrations obtained from applying the Gerchberg-Saxton algorithm on the unocculted PSF and distributed between the entrance PIAA pupil (M1) and the Inverse PIAA exit pupil (L1) in the simulation. Phase aberration RMS value is 0.4 μm.

(black dashed curve) we performed for which artificial tip/tilt was injected on the DM and the resulting contrast was measured. Although there is a discrepancy in the exact contrast level the two contrast decades per decade of residual tip/tilt is matched between between the experiment and the simulated model. Finally, we indicate the contrast levels obtained from the Test A experimental run. The SN wavefront correction algorithm was run for monochromatic input light until a 1×10^{-5} contrast level was reached in the IWZ. Then the LOWFS was turned on and the monochromatic contrast level in the IWZ improved to 3×10^{-6}. Once this level stabilized the DM settings were maintained constant, the input light bandwidth was increased to 10 %, and the corresponding broadband contrast was measured in both the IWZ and OWZ. As indicated in Figure 11 (a), these experimental contrast data points lie on the simulated sensitivity curves and give a measure of the improvement from the removal of the tip/tilt modes by the LOWFS.

We also posed the question as to whether the observed degradation in contrast performance as a function of bandwidth (as shown in the experimental bandwidth sensitivity at the end of Test C in Table 1). We computed the IWZ and OWZ median contrast by maintaining the obtained
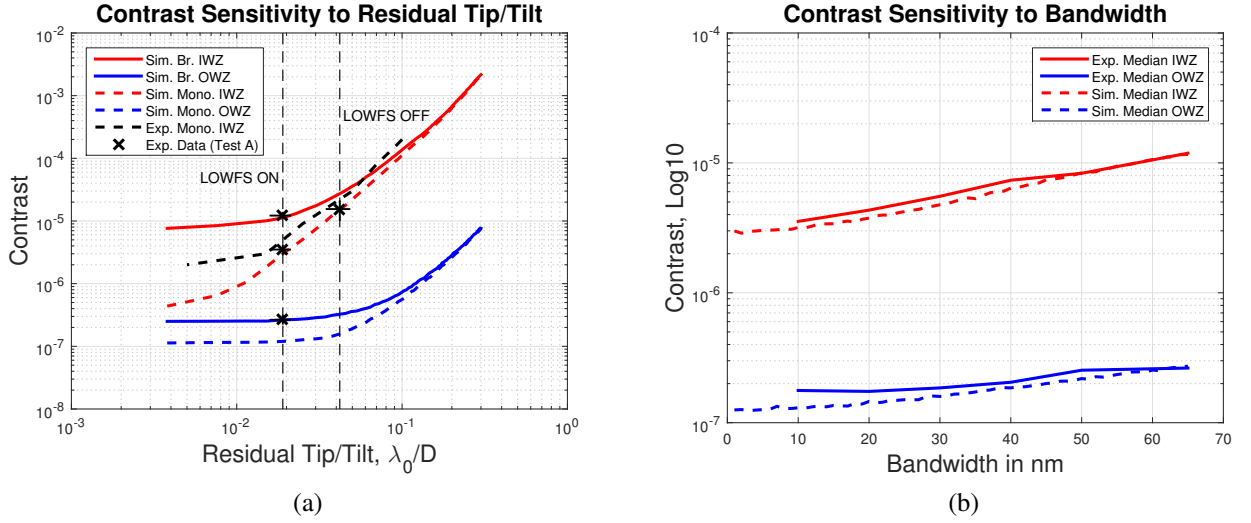
Fig 11: Contrast sensitivity analysis of model for: (a) residual tilt and (b) bandwidth size.

monochromatic DM settings gradually increasing the filter bandwidth from 10 nm (1.5%); the minimum tunable setting beyond monochromatic in our test configuration) up to 65 nm (corresponding to 10% light) or vice-versa. This was also done in simulation. The comparison is shown in Figure 11(b). For the IWZ, we have a factor of 3 degradation of contrast from 10 nm to 65 nm in the test bed that is matched by simulation. The degradation in contrast for increased bandwidths is more pronounced for the IWZ than for the OWZ.

4.4 Simulation Results

To determine the effect of the low-order aberrations on the performance of the EXCEDE starlight suppression system, we perform a simulation similar to the ideal case that established a performance baseline. In particular, we apply the low-order aberrations matched to the measured experimental PSF as described in the previous section together with $\lambda/20$ surface aberrations as expected from the optical surfaces. The result of this simulation is shown in Figure 12(a). We compare this result with experimental results, in particular a representative frame from Test A in Figure 12(b). The contrast in the IWZ is limited by diffracted light at the center of the image. The shape
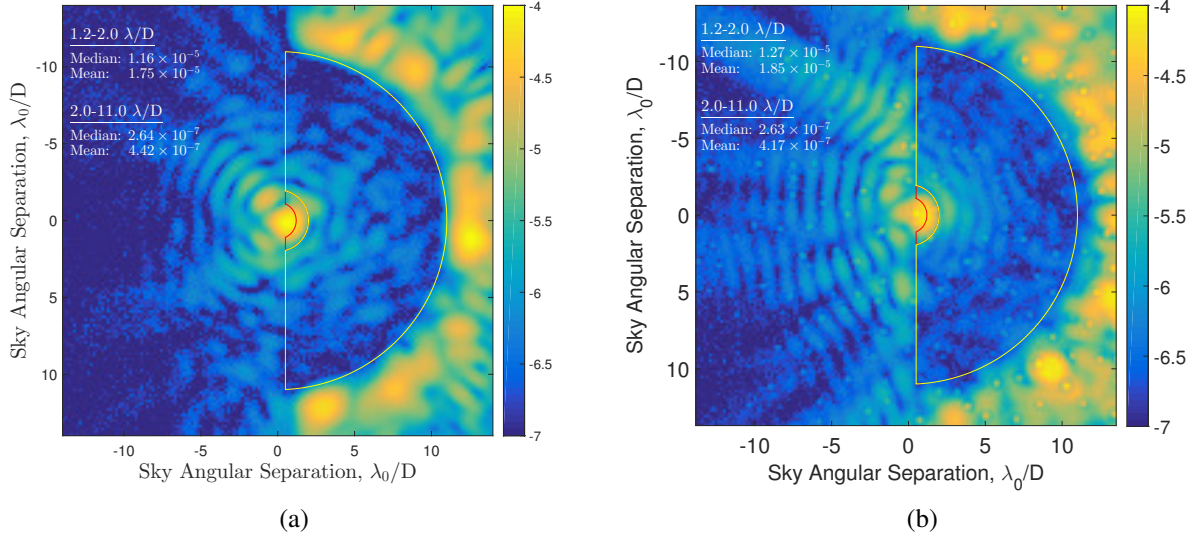
25

Fig 12: Performance comparison of the EXCEDE optical testbench between: (a) simulation results (b) experimental results.

and intensity of this diffracted light is related to the low-order aberrations present in the system upstream of the focal plane occulter (at the PIAA M1 entrance pupil plane). We can observe important qualitative similarities between the simulation and experiment. Specifically, the diffracted light centered behind in the focal plane occulter features a bright spot in the center and two dimmer companion spots. The location of the spot is matched to that of the experiment by the inner working angle verification routine – when the mask is set such that the IWA is located at 1.2 λ/D, the centroid of the simulated diffraction spot is the same as that observed in the experiment. The ringing structure around this bright spot is at a similar scale (approximately 4 Airy rings out to 5 λ/D), and this is given by matching the size of the Lyot stop between experiment and simulation. The contrast field in the OWZ contrast level is well-matched between simulation and experiment although there are some morphological differences in the speckle structure.

For a more quantitative comparison, we plot azimuthal median curves in Figure 13. We show the azimuthal median of each of the three reduced experimental tests as solid colored curves, with
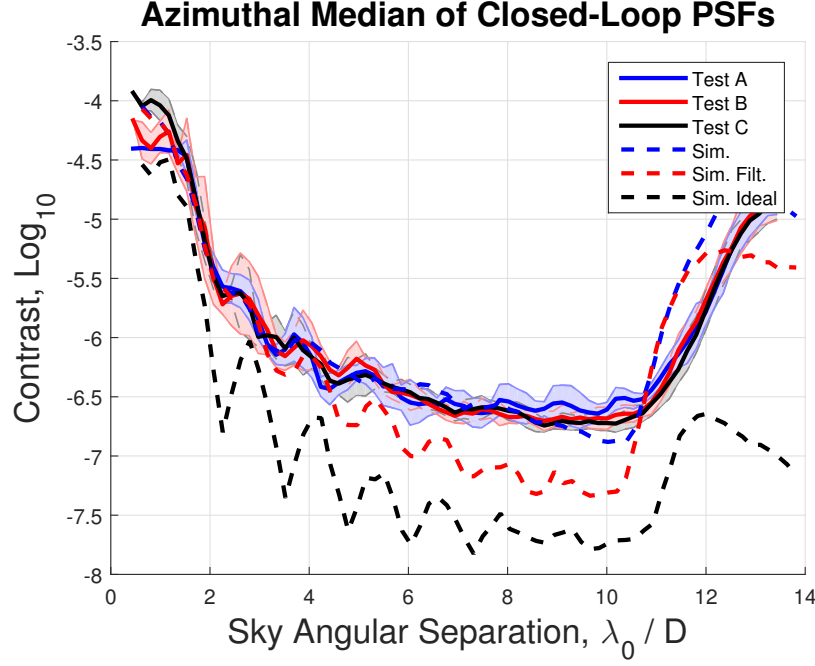
26

Fig 13: Azimuthal comparison of the median for the three experimental tests indicated by solid curves and simulation. Shaded regions represent ±15th percentile about the median for the experimental results and show contrast spread. Three simulation curves are depicted by dashed lines: the simulated ideal case represents the best-case performance attainable with this configuration, the simulated filtered case uses aberrations representing only the first 30 Zernike terms which dominate performance in the IWZ, and the combined simulation with the addition of higher mid-spatial frequency provides a good match to experimental results.

the 30th percentile population around the median indicated in the shaded region as an indicator of the contrast spread. This demonstrates the repeatability of the experiment not only in terms of the overall contrast level but also in terms of spatial distribution across the entire dark hole. The azimuthal median of the simulated system is shown via the dashed blue curve and is in good agreement with the experimental data. As an illustration of the deterioration of contrast due to the presence of low-order aberrations we have also plotted the azimuthal curve of the ideal system simulation previously shown in Figure 8.

Filtering of the phase aberrations to keep only the first 30-fitted Zernike polynomial terms maintains good agreement in the IWZ but the overall simulated contrast in the OWZ is nearly an order of magnitude better than the level observed experimentally. This indicates that, as expected,

the IWZ contrast is primarily limited by the low-order phase aberration modes with the OWZ limited by mid-spatial frequency modes. Improvements in optical alignment in vacuum to reduce low-order aberrations (for example, using a criterion that the starting Strehl Ratio should be 0.9 or better) and through estimation and correction of additional low-order modes with the LOWFS is expected to improve the IWZ contrast to approach the EXCEDE science goal of 10^{-6} raw median contrast in the IWZ.

5 Conclusions

In this paper, we have presented experimental results demonstrating wavefront control high-contrast imaging capability in 10% broadband light centered about 650 nm in vacuum for small angular separations starting at 1.2 λ/D using a highly-efficient PIAA coronagraph architecture closely approximating the conditions for the proposed EXCEDE mission. We have measured through three separate experimental runs repeatable and stable median raw contrast of 1×10^{-5} from 1.2-2.0 λ/D simultaneously with 3×10^{-7} from 2.0-11.0 λ/D. Numerical simulations of the optical model show a good match to experimental results for contrast sensitivity to the input light bandwidth and residual tip/tilt modes. We have investigated the degradation in contrast from the ideal performance case showing that the contrast in the inner working zone is limited to the observed experimental levels by low-order aberrations including tip/tilt residuals and their combination with optical errors.

The work has described results that are part of technology maturation process for the EXCEDE coronagraph, however it has significance relevant to other missions. In particular the WFIRST-AFTA PIAACMC architecture is very similar to the explored EXCEDE configuration. Additionally, through experimental verification for EXCEDE, our results explore fundamental trade-offs between contrast, inner working angle, and sensitivity to low-order aberrations and thus this work

is relevant to all Lyot-style coronagraphs helping to raise the technology readiness level for high-contrast starlight suppression.

References

1 O. Guyon, G. H. Schneider, R. Belikov, and D. J. Tenerelli, "The Exoplanetary Circumstellar Environments and Disk Explorer (EXCEDE)," *Proc. SPIE* **8442** (2012).

2 R. D. Blandford *et al.*, *New Worlds, New Horizons in Astronomy and Astrophysics*, National Academies Press (2010).

3 O. Guyon, E. Pluzhnik, R. Galicher, F. Martinache, S. Ridgway, and R. Woodruff, "Exoplanet Imaging with a Phase-induced Amplitude Apodization Coronagraph. I. Principle," *ApJ* **622** (2005).

4 O. Guyon, "Phase-induced amplitude apodization of telescope pupils for extrasolar terrestrial planet imaging," *Astronom. and Astrophys.* **404** (2003).

5 O. Guyon, E. Pluzhnik, F. Martinache, J. Totems, S. Tanaka, T. Matsuo, C. Blain, and R. Belikov, "High Contrast Imaging and Wavefront Control with a PIAA Coronagraph: Laboratory System Validation," *PASP* **693** (2010).

6 R. Belikov, E. Pluzhnik, M. S. Connelley, F. Witteborn, T. P. Greene, D. H. Lynch, P. T. Zell, and O. Guyon, "Laboratory Demonstration of High-Contrast Imaging at 2 λ/D on a Temperature-Stabilized Testbed in Air," *Proc. SPIE* **7731** (2010).

7 R. Belikov, E. Pluzhnik, F. Witteborn, T. P. Greene, D. H. Lynch, P. T. Zell, and O. Guyon, "Laboratory Demonstration of High-Contrast Imaging at 2 λ/D on a Temperature-Stabilized Testbed in Air," *Proc. SPIE* **8151** (2011).

8 O. Guyon, B. Kern, A. Kuhnert, and A. Niessner, "Phase-Induced Aodization (PIAA) Technology Development, Milestone 3," *JPL Technical Report* (2014).

9 E. Cady, C. M. Prada, X. An, K. Balasubramanian, R. Diaz, N. J. Kasdin, A. Kuhnert, B. Nemati, I. Poberezhskiy, A. J. Riggs, R. Zimmer, and N. Zimmerman, "Demonstration of high contrast with an obscured aperture with the WFIRST-AFTA shaped pupil coronagraph," *Accepted by JATIS* (2015).

10 B.-J. Seo, B. Gordon, B. Kern, A. Kuhnert, D. Moody, R. Muller, I. Poberezhskiy, J. Trauger, and D. Wilson, "Milestone 4 Final Rerpot: Narrowband Contrast Testbed Demonstration of Hybrid Lyot Coronagraph for WFIRST-AFTA," *JPL Technical Report* (2015).

11 B. Kern, "Impact of WFIRST-AFTA line-of-sight ijtter distributions on PIAACMC science yield," *In review with JATIS* (2015).

12 J. Krist, B. Nemeti, and B. Mennesson, "Numerical modelling of the proposed WFIRST-AFTA coronagraphs and their predicted performances," *Accepted by JATIS* (2015).

13 K. Balasubramanian, V. White, K. Yee, P. Echternach, R. Muller, M. Dickie, E. Cady, C. M. Prada, D. Ryan, I. Poberezhskiy, H. Zhou, B. Kern, A. Riggs, N. Zimmerman, D. Sirbu, S. Shaklan, and N. Kasdin, "Exoplanet Coronagraph Shaped Pupil Masks and Laboratory Scale Star Shade Masks: Design, Fabrication, and Characterization," *Proc. SPIE* **9605** (2015).

14 E. Pluzhnik, O. Guyon, R. Belikov, and E. Bendek, "Design of Off-Axis PIAACMC Mirrors," *Accepted by JATIS* (2015).

15 R. Belikov, E. Pluzhnik, F. Witteborn, T. P. Greene, D. H. Lynch, P. T. Zell, G. Schneider, O. Guyon, and D. Tenerelli, "EXCEDE Technology Development I: First demonstrations of high contrast at 1.2 λ/D for an Explorer space telescope mission.," *Proc. SPIE* **8442** (2012).

16 R. Belikov, E. Bendek, T. P. Greene, , O. Guyon, J. Lizi, D. H. Lynch, K. E. Newman, E. Pluzhnik, G. Schneider, D. Tenerelli, S. J. Thomas, and F. C. Witteborn, "EXCEDE Technology Development II: demonstration of high contrast at 1.2 λ/D and preliminary broadband results.," *Proc. SPIE* **8864** (2013).

17 J. Lozi, R. Belikov, G. Schneider, O. Guyon, E. Pluzhnik, S. J. Thomas, and F. Martinache, "Experimental study of the low-order wavefront sensor for the high-contrast coronagraphic imager EXCEDE.," *Proc. SPIE* **8864** (2013).

18 J. Lozi, R. Belikov, S. J. Thomsa, E. Pluzhnik, E. Bendek, O. Guyon, and G. Schneider, "Experimental study of a low-order wavefront sensor for high-contrast coronagraphic imagers: reslts in air and in vacuum.," *Proc. SPIE* **9143** (2014).

19 R. Belikov, J. Lozi, E. Pluzhnik, T. Hix, E. Bendek, S. J. Thomas, D. H. Lynch, R. Mihara, J. W. Irwin, T. P. Greene, O. Guyon, R. L. Kendrick, E. H. Smith, F. C. Witteborn, and

G. Schneider, "EXCEDE Technology Development III: First Vacuum Tests.," *Proc. SPIE* **9143** (2014).

20 D. Sirbu, S. J. Thomas, R. Belikov, J. Lozi, E. Bendek, E. Pluzhnik, D. . Lynch, T. Hix, P. Zell, G. Schneider, and O. Guyon, "EXCEDE Technology Development IV: Demonstration of Polychromatic Contrast in Vacuum at 1.2 λ/D.," *Proc. SPIE* **9605** (2015).

ban

Dan Sirbu is an NPP postdoctoral researcher at the NASA Ames Research Center and is affiliated with the Ames Coronagraph Experiment (ACE) Lab. He received his BSc in Electrical Engineering from the University of Alberta in 2008, and his PhD degree in Mechanical & Aerospace Engineering from Princeton University in 2014. His research interests are related to high-contrast imaging towards the detection and characterization of exoplanets including advanced wavefront control and estimation algorithms, internal coronagraphs and external occulters.

Sandrine Thomas is a scientist.

Ruslan Belikov is currently the head of the Ames Coronagraph Experiment (ACE) research group at NASA Ames. Under Belikov's leadership, ACE has been successfully maturing the PIAA coronagraph and wavefront control technologies, as well as pushing the state-of-the art in high contrast imaging performance at the diffraction limit. Belikov is also a member of the Exo-C mission concept Science and Technology Definition Team, takes part in the coronagraph technology development effort for the WFIRST-AFTA mission and the EXCEDE (Exoplanetary Circumstellar Environments and Disk Explorer) mission concept, and is the PI of the ACESat mission concept.

Biographies and photographs of the other authors are not available.

List of Figures

List of Tables